Desalination and Water Treatment
www.deswater.com
doi: 10.1080/19443994.2014.979243

57 (2016) 2113–2124
January

Taylor & Francis
Taylor & Francis Group

The precipitation of fluoride, calcium and magnesium minerals from Egyptian Mediterranean Sea coast in relation to discharged waters

Ghada F. El-Said[a,*], Nayrah A. Shaltout[b], Abeer A. Moneer[a], Manal M. El-Sadaawy[a], Amal M.H. Morsy[a]

[a]*Marine Pollution Laboratory, Environmental Division, National Institute of Oceanography and Fisheries, Kayet Bay, El-Anfoushy, Alexandria, Egypt, Tel. +20 1220607816; Fax: +20 34801499; +20 34801553; +20 34801174; emails: ghadafarouk25@yahoo.com, gfarouk66@hotmail.com (G.F. El-Said), yrwah@yahoo.com (A.A. Moneer), manal_dn@yahoo.com (M.M. El-Sadaawy), amalmorsy2014@yahoo.com (A.M.H. Morsy)*

[b]*Marine Chemistry Laboratory, Environmental Division, National Institute of Oceanography and Fisheries, Kayet Bay, El-Anfoushy, Alexandria, Egypt, email: nshaltout@gmail.com*

Received 26 April 2014; Accepted 16 October 2014

ABSTRACT

The present study focuses on the effect of discharged wastes on the precipitation of some minerals (calcite, aragonite, dolomite, fluorite and sellaïte) as well as the chemical composition of seawater water columns along the eastern Egyptian Mediterranean Sea coast. This coast is subjected to different discharge waters containing agricultural, industrial, sewage and domestic wastes coming from the Nile River, the North Lakes as well as other different outlets. Variable levels of physicochemical parameters including temperature (*T*; 15.34–23.12˚C), salinity (38.50–40.33‰), pH (8.05–8.31), bicarbonate (HCO_3; 63.73–147.22 mg/l), carbonate (CO_3; 10.01–23.34 mg/l), calcium (Ca; 263.68–791.05 mg/l), magnesium (Mg; 799.67–2452.32 mg/l) and fluoride (F; 0.56–4.76 mg/l) were measured. Amongst the mineral production values that were calculated by saturation index (SI), fluorite and sellaïte calculations almost showed values <1, especially in the Rosetta and Damietta sectors which are affected by the Nile River. Marine organisms were influenced by the change in the physicochemical parameters along the investigated coastal area and showed aragonite and high-Mg calcite formation. Obviously, the statistical analyses of correlation matrix, ANOVA: two-factor without replication and stepwise regression of the present data explored the effect of the discharged effluents on the minerals formation and the chemical composition of seawater along the studied area. Additionally, the results showed the possible public health hazard from marine organism's ingestion and seawater contact along the polluted areas. Accordingly, it seems advisable to reduce the pollution by discharged wastes into the Egyptian coastal ecosystems.

Keywords: Water columns; Physicochemical parameters; Molar Mg/Ca; Minerals; Saturation index; Eastern Egyptian Mediterranean Sea coast

*Corresponding author.

This article was originally published with errors. This version has been corrected. Please see Corrigendum (http://dx.doi.org/10.1080/19443994.2015.1014986).

1. Introduction

The behaviour of some seawater's mineral constitutes is affected by both untreated discharged waters and different outlets that fall along the coastal zones [1]. Water contacting with rock forms minerals with considerable amounts and different ions in the solution. The effect of such ions or the so-called ionic strength on mineral dissolution rates was studied [2]. Recalling that, large number of works has shown the growth and dissolution rates of the ionic minerals which are influenced by the ratio of anion to cation concentrations in the solution [3,4]. For example, fluorite is the most important fluorine bearing mineral phase in the Earth's crust that control the fluoride (F^-) concentration in seawater and in other natural aqueous solutions [5]. Fluoride can interact with some seawater constituents and causes adverse effects on the marine ecosystem due to the formation, precipitation and dissolution of some mineral forms [1]. Fluorine is a reactive element which can combine practically with all of the inorganic and organic compounds [6,7]. In minerals and water, fluorine occurs as fluoride ions (F^-), which are released into aqueous solutions during weathering processes. The average fluorine concentration in the crust is estimated at 0.05–0.1% or 500–1,000 mg/kg and ranks 13th among the elements [7]. The primary fluoride sources for waters are fluorite (CaF_2), cryolite (Na_3AlF_6), fluorapatite ($Ca_5(PO_4)_3F$) and apophyllite. Also, the OH^--bearing minerals such as micas (biotite, phlogopite, lepidolite, etc.) as well as amphiboles contain high levels of fluorine (0.2–1.1%) can contribute to fluorides in water [8]. Recalling that, fluoride can replace OH^- in the Ferromagnesian silicates (amphiboles and micas), and clay minerals [9,10]. Fluoride is an essential component for the normal mineralization of bones and the formation of dental enamel [7]. On the other hand, the anthropogenic fluoride contamination of seawater is mainly accompanied with mineral processing industries such as coal-fired power station, beryllium extraction plants, brick and iron works and aluminium smelter [11]. Acute oral exposure to fluoride may cause nausea, vomiting, abdominal pain, diarrhea, fatigue, drowsiness, coma, convulsions, cardiac arrest and even death [7]. Also, fluoride possibly produces calcification of muscles, osteosclerosis as well as decreases the production of erythrocytes in the long-term exposure. Additionally, it can affect the physiological processes including metabolism, growth and reproduction [12,13].

The seeded crystals and microscopic growth rate measurements showed the significant kinetic dependence of calcite on solution stoichiometry [14]. Calcite and carbonate minerals are major constituents of sedimentary rocks on the earth surface, comprising approximately 20% of them [2]. Understanding the mechanisms of their dissolution is essential for the modelling of geochemical cycles [15] and more recently for modelling systems for CO_2 storage [16]. Calcite occurs as inorganic and biogenic precipitates in both nature and anthropogenic systems [14]. However, calcite dissolution rates are influenced by the presence of dissolved organic species, including sedimentary in basins and marine ecosystem during carbon storage processes as well as the Earth's surface during the procedures of both chemical weathering and bio-mineralization [17].

Dolomite ($CaMg(CO_3)_2$) is considered as an unusual, metastable mineral, and its chemical properties behaviour should be put in context with other, most important carbonate minerals: calcite ($CaCO_3$) and magnesite ($MgCO_3$; [18]). The crystal structure of magnesite resembles the calcite one, and then magnesite properties are similar to those of calcite. Dolomite is thermodynamically unstable, and the dedolomitisation in alkaline media is represented by the following reaction [19]:

$$CaMg(CO_3)_2 + Ca(OH)_2 = 2CaCO_3 + Mg(OH)_2$$

The reverse process of dolomitisation occurs during the evaporation of seawater and its kinetics is affected by the simultaneous action of H^+, H_2CO_3 and H_2O [20].

This study concentrates on the factors affecting the mineral composition of calcite, aragonite, dolomite, fluorite and sellaïte in some hot spots regions along the eastern Egyptian Mediterranean Sea coast.

2. Materials and methods

2.1. Description of study area

Six perpendicular sectors, namely Rosetta, El-Burullus, Damietta, Port Said, El-Bardaweel and El-Arish were selected to represent the eastern Egyptian Mediterranean Sea coast (Fig. 1 and Table 1). These sectors are influenced by the discharged waters containing agricultural, industrial, domestic and sewage wastes (Table 1).

2.2. Sampling and physicochemical parameters determination

A total of 97 seawater samples were collected from the six sectors in the area of study during 5–7 May 2013 by El Yarmouk ship (R/V). These samples were

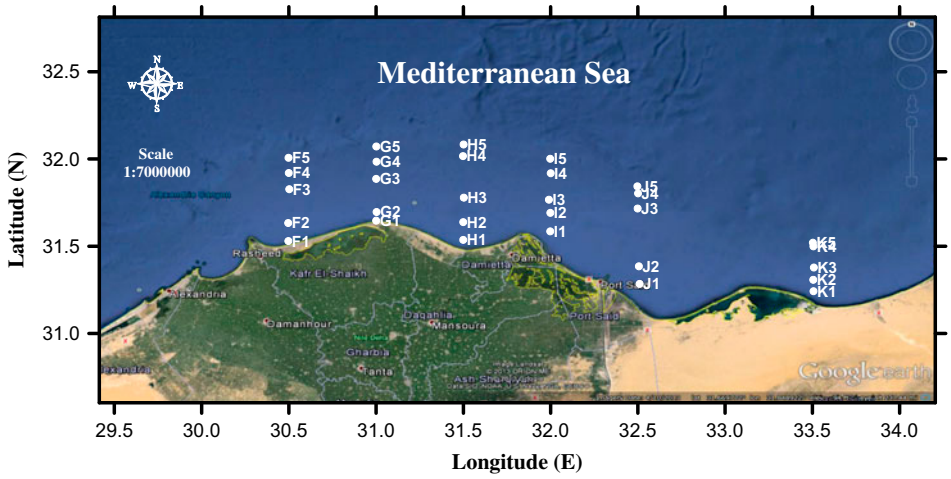

Fig. 1. Sampling locations for the investigated area.

Table 1
The description of sampling sectors along the eastern coast of the Egyptian Mediterranean Sea

Sector	Station	Longitude (E)	Latitude (N)	Depth (m)	Pollution sources
Rosetta	F5	30.4979	32.0068	0–200	Outlet of Nile River discharge agricultural, domestic and industrial wastes
	F4	30.4996	31.9196	0–100	
	F3	30.5022	31.8267	0–50	
	F2	30.4961	31.633	0–20	
	F1	30.4970	31.5297	0–10	
El-Burullus	G5	31.0011	32.0715	0–200	Mainly agriculture drainage water
	G4	31.0021	31.9841	0–100	
	G3	31.0001	31.8859	0–50	
	G2	31.0026	31.696	0–20	
	G1	31.0003	31.6466	0–10	
Damietta	H5	31.5011	32.0829	0–200	Raw sewage, agricultural and industrial effluents
	H4	31.4979	32.0164	0–100	
	H3	31.5025	31.7783	0–50	
	H2	31.4993	31.6381	0–20	
	H1	31.4990	31.5363	0–10	
Port Said	I5	31.9975	32.0011	0–200	Industrial, agricultural, sewage and commercial wastes from Lake Manzala
	I4	32.0005	31.9181	0–100	
	I3	31.9901	31.7666	0–50	
	I2	31.9983	31.6912	0–20	
	I1	31.9977	31.5851	0–10	
El-Bardaweel	J5	32.4970	31.8433	0–200	
	J4	32.5009	31.8030	0–100	
	J3	32.4986	31.7161	0–50	
	J2	32.5058	31.3849	0–20	
	J1	32.5102	31.2843	0–10	
El-Arish	K5	33.5028	31.5202	0–200	Public beach and flash flood water from the north and the central of Sinai [56]
	K4	33.5055	31.4993	0–100	
	K3	33.5085	31.3779	0–50	
	K2	33.5051	31.3076	0–20	
	K1	33.5064	31.2423	0–10	

gathered from different depths (surface to 200 m) along five stations in each sector. The samples were preserved in clean polyethylene bottles and then immediately were frozen at −20˚C. The frozen samples were transferred to the National Institute of Oceanography and Fisheries and kept frozen at −20˚C. Fluoride ion concentration was determined by the colorimetric procedure of zirconium alizarin red S [21,22] using a UV–visible single beam Spectronic 21 D Milton Roy spectrophotometer. Calcium and magnesium were determined by EDTA titration in the presence of murexide and Eriochrome black T indicators, respectively [23]. Total alkalinity was measured using a potentiometric titration with an open cell system [24]. TA calibration was carried out using certified reference material CRM batch 15 provided by Dickson. The pH was measured on a total scale using pH ± 0.02 (Jenway Model 3505 pH) using tris-buffer. Carbonate and bicarbonate concentration were calculated by applying CO_2SYS to inorganic carbon system parameters (CO_3, HCO_3, Ω_{Cal}, Ω_{arg}). Salinity and temperature at the different water column depths were measured by CTD-Sea-Bird 19plus.

2.3. Saturation index calculation

The saturation index (SI) for the minerals of fluoride, calcium and magnesium was calculated as the product of the molar concentrations of the component ions divided by its equilibrium solubility constant (K_{sp}) [25]. The calculated K_{sp} values of calcite, aragonite, dolomite, fluorite and sellaïte were 3.36×10^{-9}, 6.0×10^{-9}, 1×10^{-11}, 3.45×10^{-11} and 5.16×10^{-11}, respectively [26]. However, SI < 1 indicates that the water is under saturated with respect to that particular mineral. Whereas, SI > 1 specifies that water is oversaturated with respect to the particular mineral and therefore incapable of dissolving more.

2.4. Statistical analyses

The statistical analyses of the correlation matrix and multiple regression equations for the data were done using Statistica version 5.0. The ANOVA: two factor without replication was conducted with Microsoft Office Excel 2007. Statistical analyses were applied among the determined parameters of temperature, salinity, pH, bicarbonate, carbonate, calcium, magnesium, fluoride and the SI of minerals (calcite, aragonite, dolomite, fluorite and sellaïte). Moreover, r (correlation coefficient) and R (multiple regression coefficient) values were measured at a significant level of $\alpha = 0.05$.

3. Results and discussion

3.1. Physicochemical parameters

The distributed levels and the horizontal and vertical patterns of the measured physical parameters including temperature and salinity along the studied area are shown in Figs. 2 and 3. The minimum and maximum temperatures 15.34 and 23.12˚C are recorded at 200 m in Rosetta and at the surface in El-Bardaweel, respectively. The vertical variation of temperature shows a gradual decrease from the surface to 200 m depth which is characterized by low temperature values at El-Burullus and El-Bardaweel sectors (Fig. 3). The salinity ranges from 38.50 to 40.33‰ at the surface of station F1 (Rosetta sector) and the 20 m of station J2 (El-Bardaweel), respectively. The horizontal and vertical distribution patterns of salinity give a gradual decrease from the eastern to the western sides (Figs. 2 and 3). The high salinity values are recorded along El-Bardaweel and El-Arish sectors. This observation is related to the huge discharge waters falling into seawater from Rosetta, El-Burullus, Damietta and from the different outlets in the investigated region [27].

3.2. Chemical parameters

The different chemical parameters of pH, bicarbonate (HCO_3^-), carbonate (CO_3^{-2}), calcium (Ca^{+2}), magnesium (Mg^{+2}) and fluoride (F^-) are determined (Table 2). The pHs show relatively similar values ranging from 8.05 to 8.31. The high pHs are detected at the eastern and the western district of the area under investigation, however, the low pHs are detected in Port-Said and El-Bardaweel sectors (Figs. 2 and 3). Generally, pH values attribute to aquatic environmental factors such as photosynthetic activity and respiration of aquatic organisms, decomposition of organic matter, precipitation, dissolution, temperature, salinity and oxidation–reduction reactions [28], that is, besides the discharge of fresh water with low pH at these sites. The lower values near the bottom reflect the dissolution of $CaCO_3$ from the sediment and the respiration of marine organisms [29]. Meanwhile, the higher ones at the top of the water column may be attributed to the uptake of CO_2, the precipitation of $CaCO_3$ and photosynthesis of marine plants.

Bicarbonate and carbonate fluctuate from minimums 63.73 and 10.01 and maximums 144.64 and 23.34 mg/l along the different sectors, respectively (Table 2). They show drastically different distributions with relatively similar horizontal and vertical patterns along the studied area (Figs. 2 and 3). The high levels

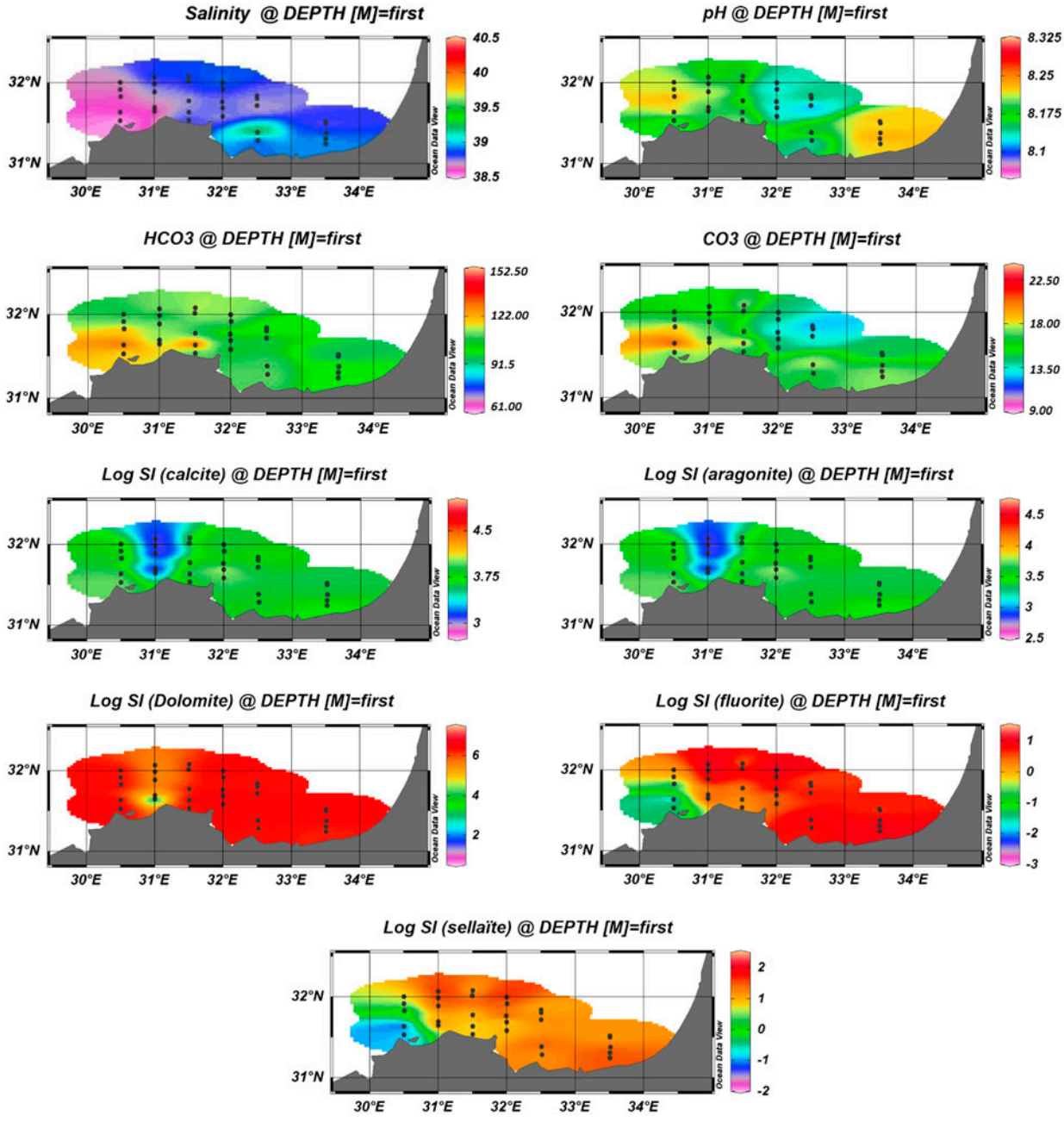

Fig. 2. Horizontal distribution of the physicochemical parameters and saturation index (SI) of minerals in surface water along the eastern Egyptian Mediterranean Sea coast.

are recorded in Rosetta and El-Arish sectors. The horizontal patterns of bicarbonate and carbonate contents have similar relative distribution to the pH levels along the studied region (Fig. 2) and pH and carbonate and carbonate and bicarbonate show high significant relations ($r = 0.546$; $p < 0.005$ and $r = 0.632$; $p < 0.005$, respectively; Table 3), recalling that calcium carbonate dissolves in an acidic medium [14]. Also, the measured carbonate content has a high significant relation with temperature values ($r = 0.340$; $p < 0.005$), reflecting the decrease in the precipitation of $CaCO_3$ in low temperatures [17].

The minimum and maximum calcium and magnesium contents range between 263.68 and 799.67 and 791.05 and 2,452.33 mg/l, respectively (Table 2). However, the lowest calcium level (263.68 mg/l) is detected at 20 m of station J5 in El-Bardaweel and the maximum ones are recorded at El-Burullus, El-Bardaweel

Table 2
The distribution of the determined parameters and saturation index (SI) of minerals along the eastern coast of the Egyptian Mediterranean Sea

Sector	Station	pH	HCO_3^- (mg/l)	CO_3^{-2} (mg/l)	Ca^{+2} (mg/l)	Mg^{+2}(mg/l)	mMg/Ca	F^- (mg/l)	SI (Calcite)	SI (Aragonite)	SI (Dolomite)	SI (Fluorite)	SI (Sellaite)
Rosetta	F5	8.18–8.25	69.47–118.14	13.78–17.06	439.47–615.26	1599.34–1919.21	4.91–6.87	0.67–1.83	3.76–3.95	3.51–3.70	6.29–6.47	−0.25–0.55	0.29–1.08
	F4	8.18–8.25	95.32–120.73	14.48–18.33	439.47–527.37	1812.59–1919.21	5.73–6.87	0.68–1.48	3.71–3.89	3.46–3.64	6.23–6.42	−1.09–0.29	−0.51–0.95
	F3	8.20–8.29	97.44–144.64	17.46–21.30	439.47–703.16	1705.96–2132.46	5.05–6.47	0.56–0.91	3.72–4.03	3.47–3.78	6.24–6.56	−2.63–0.05	−2.00–0.53
	F2	8.22–8.24	127.56–131.71	19.35–23.34	527.37–703.16	1919.21–2025.83	4.80–6.07	0.59–0.61	3.94–4.04	3.69–3.79	6.47–6.57	−2.42–1.34	−1.92–0.74
	F1	8.09–8.21	106.15–125.49	13.14–20.23	703.16–703.16	1332.79–2132.46	3.16–5.05	0.60–0.57	3.96–4.03	3.71–3.78	6.49–6.56	−2.17–0.55	−1.86
Average ± SD			113.90 ± 14.08	17.25 ± 2.61	561.55 ± 91.14	1830.36 ± 184.68	5.54 ± 0.86	1.10 ± 0.38	3.88 ± 0.10	3.63 ± 0.10	6.41 ± 0.10	−0.52 ± 1.00	0.04 ± 1.01
El-Burullus	G5	8.15–8.21	89.66–124.80	14.37–16.68	439.47–791.05	1865.90–2132.46	4.27–7.08	1.93–4.76	2.91–3.17	2.66–2.92	5.44–5.70	0.52–1.50	1.19–2.03
	G4	8.19–8.2	97.85–111.60	13.40–17.02	439.47–615.26	1652.65–2079.15	5.20–6.40	2.72–3.86	2.94–3.10	2.70–2.84	5.47–5.62	0.90–1.27	1.52–1.84
	G3	8.16–8.31	63.73–141.32	12.41–23.24	351.58–791.05	1226.16–1812.59	3.82–6.47	2.48–3.86	2.83–3.22	2.58–2.97	5.36–5.75	0.73–1.12	1.32–1.76
	G2	8.18–8.21	103.01–121.29	16.73–17.50	439.47–703.16	2239.08–2452.33	5.81–8.49	1.03–2.59	2.97–3.18	2.72–2.93	5.50–5.71	−0.03–0.85	0.73–1.53
	G1	8.18	120.26	18.71	527.37	1812.59	5.73	2.59	3.09	2.84	0.99	0.85	1.43
Average ± SD			110.59 ± 16.46	16.03 ± 2.36	564.38 ± 125.39	1961.30 ± 273.33	5.96 ± 1.03	2.86 ± 0.91	3.04 ± 0.10	2.78 ± 0.10	5.32 ± 1.05	0.90 ± 0.36	1.50 ± 0.32
Damietta	H5	8.17–8.23	101.67–120.26	14.03–19.15	351.58–527.37	1705.97–2025.83	5.39–8.09	0.97–1.69	3.65–3.88	3.40–3.63	6.18–6.40	0.01–0.3	0.63–1.04
	H4	8.18–8.21	124.21–147.22	17.36–22.00	615.26–615.26	1865–90-1919.21	5.05–5.20	1.03–1.24	3.97–4.04	3.72–3.79	6.50–6.57	0.12–0.28	0.66–0.81
	H3	8.14–8.21	105.60–108.84	14.52–15.79	439.47–527.37	1812.59–1865.90	5.73–7.08	1.17–1.48	3.77–3.83	3.51–3.58	6.29–6.36	0.08–0.37	0.76–0.95
	H2	8.19	115.27	18.11	527.37	1865.90	5.9	1.97	3.87	3.62	6.40	0.61	1.21
	H1	8.20	115.86	18.94	439.47	1332.79	5.05	1.34	3.79	3.54	6.32	0.20	0.73
Average ± SD			155.63 ± 13.84	17.26 ± 2.57	507.84 ± 85.42	1788.89 ± 197.88	7.14 ± 1.03	1.35 ± 0.32	3.85 ± 0.12	3.59 ± 0.12	6.37 ± 0.12	0.24 ± 0.17	0.84 ± 0.18
Port Said	I5	8.08–8.18	107.05–120.36	12.01–15.83	439.47–615.26	1546.03–2292.39	5.49–6.87	2.52–4.14	3.77–3.96	3.52–3.70	6.30–6.48	0.83–1.28	1.41–1.85
	I4	8.10–8.16	94.50–121.38	13.26–14.65	351.58–615.26	1812.59–2132.46	5.78–8.59	1.69–3.80	3.72–3.96	3.46–3.70	6.24–6.48	0.54–1.18	1.13–1.84
	I3	8.11–8.15	91.21–104.09	12.13–14.15	439.47–527.37	1599.34–1919.21	6.07–7.28	2.38–3.93	3.69–3.80	3.44–3.54	6.22–6.32	0.70–1.13	1.39–1.80
	I2	8.10–8.13	101.11–119.06	12.81–15.43	439.47–527.37	2079.14–2185.77	6.74–7.88	0.90–0.97	3.85–4.81	3.60–4.55	6.38–7.33	−0.07–0.92	0.57–0.66
	I1	8.12–8.13	97.25–107.58	13.72–14.39	703.16–703.16	1812.59–2185.77	4.30–5.18	1.29–1.78	3.92–3.97	3.67–3.71	6.45–6.49	0.37–0.65	0.83–1.19
Average ± SD			107.85 ± 9.76	13.89 ± 1.22	527.37 ± 97.17	1966.91 ± 206.39	6.35 ± 0.98	2.58 ± 1.09	3.89 ± 0.24	3.64 ± 0.24	6.42 ± 0.24	0.80 ± 0.38	1.37 ± 0.43
El-Bardaweel	J5	8.13–8.16	91.14–106.84	11.68–13.04	263.68–791.05	799.67–1759.28	2.02–11.12	1.26–2.31	3.50–4.01	3.25–3.76	6.03–6.54	0.05–0.88	0.53–1.32
	J4	8.10–8.18	91.22–107.66	10.01–15.38	351.58–615.26	1119.54–1759.28	3.61–8.34	1.05–3.33	3.66–3.88	3.41–3.63	6.19–6.41	0.14–1.14	0.61–1.52

	J3	8.05–8.14	105.85–113.39	12.69–14.13	439.47–703.16	1012.92–1865.90	2.40–7.08	2.14–2.55	3.75–3.99	3.50–3.74	6.28–6.51	0.61–0.87	1.02–1.38
	J2	8.16–8.22	102.33–122.30	16.91–19.13	351.58–703.16	852.98–1759.28	2.02–7.32	1.88–4.29	3.64–3.96	3.39–3.71	6.17–6.49	0.70–1.11	0.83–1.80
	J1	8.05–8.20	106.71–114.43	13.73–18.02	439.47–527.37	1119.54–1546.03	3.54–5.86	1.60–3.12	3.76–3.87	3.51–3.62	6.28–6.39	0.36–1.01	0.95–1.39
Average ± SD			103.32 ± 8.10	13.93 ± 2.35	531.76 ± 141.08	1394.09 ± 339.06	4.85 ± 2.30	2.32 ± 0.79	3.81 ± 0.14	3.56 ± 0.14	6.34 ± 0.14	0.69 ± 0.32	1.16 ± 0.33
El-Arish	K5	8.20–8.25	93.31–107.72	14.33–15.56	615.26–791.05	1652.65–1759.28	3.48–4.77	1.78–2.47	3.85–4.02	3.60–3.77	6.38–6.54	0.59–0.98	1.09–1.35
	K4	8.18–8.21	87.94–90.13	12.32–13.87	527.37–703.16	1812.59–1812.59	5.73–4.30	1.47–1.57	3.76–3.88	3.51–3.63	6.29–6.40	0.42–0.48	0.94–1.00
	K3	8.20–8.26	95.02–111.78	15.46–18.17	615.26–615.26	1546.03–1759.28	4.19–4.77	2.47–2.64	3.85–3.92	3.60–3.67	6.38–6.45	0.88–0.93	1.32–1.44
	K2	8.21–8.27	93.97–105.45	14.65–20.59	527.37–527.37	1386.10–1492.72	4.38–4.72	2.91–3.84	3.78–3.83	3.53–3.58	6.31–3.36	0.95–1.19	1.45–1.66
	K1	8.21–8.22	97.28–101.38	17.26–17.66	351.58–439.47	1172.85–1652.65	5.56–6.27	2.88–3.47	3.62–3.74	3.37–3.48	6.15–6.26	0.86–0.93	1.49–1.50
Average ± SD			97.88 ± 7.63	15.89 ± 2.58	593.29 ± 130.50	1626.00 ± 194.89	4.71 ± 0.83	2.46 ± 0.74	3.84 ± 0.11	3.59 ± 0.11	6.36 ± 0.11	0.80 ± 0.23	1.30 ± 0.22

and El-Arish sectors (791.05 mg/l, Table 2). Meanwhile, the minimum (799.67 mg/l) and maximum (2,452.33 mg/l) contents of magnesium are determined at 100 m in station J5 sector El-Barrdaweel and 20 m in station G2 sector El-Burullus, respectively. It seems from the present study that the concentrations of calcium and magnesium are variable and differ from those recorded for open seawater (412 and 1,294 mg/l, respectively; [30]). This possibly relates to discharged waters, the formation and dissolution of minerals, pH value, CO_2 level, phototropic species, presence of potassium and sodium salts that increase $CaCO_3$ solubility, as well as the reaction of phosphate ion with Ca^{+2} to form calcium phosphate [28,31,32]. The significant positive correlation between magnesium and bicarbonate ($r = 0.246$; $p < 0.05$; Table 3) indicates that the dissociation of hydrated carbon dioxide is accompanied with magnesium ions in the seawater column [28]. El-Said [31] detected higher calcium and magnesium contents (549.7 ± 63.2 and 1349.7 ± 204.0 mg/l, respectively) in 2011 than those documented for open seawater [30].

The seawater molar magnesium calcium ratio (mMg/Ca) views the growth of calcitic vs. aragonitic marine organisms and the deposition of inorganic carbonates as well as the status of ocean–atmosphere CO_2 exchange [33,34]. Also, abiogenic carbonates precipitated from seawater is affected by several factors, including temperature, precipitation rate, fluid inclusions, amorphous calcium carbonate precursors, ion attachment/detachment kinetics, surface entrapment and Mg speciation [35]. However, the polymorph mineralogy of $CaCO_3$ that precipitated abiotically from seawater is determined by the molar ratio of Mg/Ca (mMg/Ca < 2 = calcite; mMg/Ca > 2 = aragonite + high-Mg calcite) with a range of 1.0–5.2 over Precambrian time. The determined mMg/Ca in the present work shows values >2 (2.02–11.12; Table 2), indicating the formation of aragonite and high-Mg calcite in the marine organisms in the investigated area. However, the highest average of mMg/Ca ratio is recorded in Damietta sector (7.14 ± 1.03); and the lowest average value is determined in El-Arish location (4.71 ± 0.83).

Fluoride varies from 0.56 to 4.76 mg/l at 50 m of F3 and at 200 m in Rosetta and in G5 of El-Burullus, respectively (Table 2). Almost all the presented sectors give fluoride concentrations differ from the reported levels for unpolluted seawaters (1.2–1.5 mg/l; [13]), except Rosetta and Damietta regions, due to the fresh water discharged from the Nile River through these branches containing the contaminated wastes. It seems from the present results that fluoride adsorbs and dissolutes near the bottom of the Mediterranean Sea,

Table 3
Correlation matrix of the determined physicochemical parameters and saturation index (SI) of minerals

Parameter	pH	T (°C)	Salinity	HCO_3	CO_3	Fluorite	Sellaite	Calcite	Aragonite	Dolomite	F	Ca	Mg
pH	1.000												
T (°C)	−0.052	1.000											
Salinity	−0.111	0.157	1.000										
HCO_3	−0.117	−0.104	−0.013	1.000									
CO_3	**0.546**	**0.340**	0.019	**0.632**	1.000								
Fluorite	**−0.286**	−0.068	**0.366**	*−0.242*	**−0.408**	1.000							
Sellaïte	*−0.258*	−0.056	**0.351**	*−0.221*	**−0.372**	**0.978**	1.000						
Calcite	−0.174	0.018	0.051	0.049	−0.046	**−0.277**	**−0.370**	1.000					
Aragonite	−0.173	0.019	0.051	0.048	−0.046	**−0.278**	**−0.371**	**1.000**	1.000				
Dolomite	−0.101	−0.078	0.127	−0.044	−0.119	−0.191	−0.247	**0.688**	**0.688**	1.000			
F	−0.190	−0.028	0.356	−0.175	**−0.268**	**0.832**	**0.853**	**−0.414**	**−0.414**	**−0.264**	1.000		
Ca	−0.030	−0.210	0.033	0.112	−0.038	−0.017	−0.118	0.176	0.176	0.113	−0.109	1.000	
Mg	0.031	−0.137	−0.042	**0.246**	0.117	−0.113	−0.024	−0.181	−0.182	−0.112	−0.088	0.140	1.000

Note: Italic font: significant $p < 0.05$. Bold font: highly significant $p < 0.005$.

especially at the sediment water interface. Indeed, the sediments of the Rosetta sector; the western part of the Nile Shelf is mainly composed of aragonite, calcite and apatite minerals [36]. The replacement of fluoride with hydroxide ions in some minerals near the seafloor may explain the low F^- concentrations (1.10 ± 0.38 mg/l; Table 2) along the water columns of the stations of Rosetta sector [37]. However, it was recorded that fluoride can replace the hydroxyl group in hydroxyapatite [38]. Also, Fluoride concentrations are governed by adsorption equilibria on sediment and by fluorite solubility. However, the ion exchange reaction can be expressed as follows [39,40]:

$$CaCO_3(s) + 2F^-(aq) = CaF_2(s) + CO_3^{-2}(aq)$$

High average fluoride concentrations recorded in El-Burullus, El-Bardaweel, Port Said and El-Arish sectors may be related to the solubility of fluoride minerals in the presence of high carbonate contents and the discharged waters containing the agricultural, industrial and sewage wastes (Tables 1 and 2). The previous works showed higher fluoride contents of 1.36–3.10, 1.39–12.90, 2.36–12.9 and 5.8–6.8 mg/l along the Egyptian Mediterranean Sea coast during 1996, 2000–2001, 2006 and 2011, respectively [31,41,42], than that reported for unpolluted areas (1.2–1.5 mg/l; [13]). The high fluoride levels can be accumulated by marine organisms in soft and hard tissues leading to many physiological effects to these organisms and finally to death. Additionally, the increase in fluoride in seawater possibly causes adverse effects on human health from the consumption of the gathered fish, bivalve, crabs, shrimp and gastropod species [13,42–45].

3.3. Mineral species precipitation

Saturation indices of calcite, aragonite, dolomite, fluorite and sellaïte minerals are calculated (Table 2). It seems from the estimated values and horizontal and vertical patterns of the log saturation indices that calcite, aragonite and dolomite species are formed (SI > 1) along the water columns of the investigated region (Figs. 2 and 3). They have ranges of 2.83–4.81, 2.58–4.55 and 0.99–7.33, respectively (Table 2). El-Burullus sector shows minimum precipitations of calcite, aragonite and dolomite with saturation indices averages of 3.04 ± 0.10, 2.78 ± 0.10 and 5.32 ± 1.05, respectively (Table 2 and Figs. 2 and 3). This possibly relates to the huge discharged waters which contain agricultural, industrial,domestic and sewage contaminants. Meanwhile, seawater is known to be practically

saturated with respect to calcium carbonate in the form of calcite and aragonite. This fact is in agreement with some observations on the super saturation with $CaCO_3$ [14,46]. The degree of super saturation is controlling with the thermodynamics and kinetics of growth processes of calcite as well as the influence of the Ca^{+2}:CO_3^{+2} activity ratio [47]. There is a relationship involving the CO_2–HCO_3^-–CO_3^{-2} equilibrium, water and hydrogen ion concentration [28]. This relation is affected by different factors including phototropic species, pH, temperature, some ions such as calcium, magnesium, sodium and potassium, some minerals, for example, the minerals of fluoride, sulphate and silicate and sedimentary beds containing minerals in the marine origin [28]. Moreover, fluorite and sellaïte minerals can be formed in all the sectors except Rosetta and Damietta ones that give SI < 1 with averages of (-0.52 ± 1.00 and 0.24 ± 0.17) and (0.04 ± 1.01 and 0.84 ± 0.18), respectively (Table 2). These fluoride minerals seem to be in equilibrium with their ionic species in the two previously mentioned sectors which are in front of the two branches of the Nile River. It was recorded that the chemistry of seawater in estuaries is dominated by river's one (fresh water) at which the ion pair of fluoride with magnesium is not as strong as the tendency to form complexes with other elements such as aluminium and thorium [48]. However, 51% of fluoride ion exists in seawater in the free form (F^-) and the remaining ones make ion pairs with magnesium (MgF^+) and calcium (CaF^+) with percentages of 46 and 2, respectively [49]. Accordingly, the horizontal and vertical distributions for both fluorite and sellaïte minerals have trends similar to the salinity and pH ones (Figs. 2 and 3), since they give high negative and positive correlations with pH ($r = -0.286$, $p < 0.05$ and $r = -0.258$, $p < 0.005$, respectively) and salinity ($r = 0.366$, $p < 0.005$ and $r = 0.351$, $p < 0.005$), respectively (Table 3). Also, the present results reflect the possible dissolution and formation of fluorite and sellaïte minerals in the presence of carbonate and bicarbonate species [40] by their significant relations ($r = -0.408$, $p < 0.005$ and $r = -0.372$, $p < 0.005$, respectively; Table 3). Additionally, the previous relations are confirmed by the significant negative relationships of F and CO_3, fluorite and CO_3, sellaïte and CO_3, F and calcite, F and aragonite and F and dolomite (Table 3). The high negative relations of fluorite and calcite, fluorite and aragonite, sellaïte and calcite and sellaïte and aragonite show high negative relations ($r = -0.277$, $r = -0.278$, $r = -0.370$ and $r = -0.371$, respectively; Table 3) which may be accompanied with the adsorption and simultaneous co-precipitation processes of fluoride with carbonate minerals by ion exchange or surface chemical reaction [50]. Additionally, this reverse relation between fluorite and carbonate minerals possibly related to the adsorption equilibria onto sediment surface and by fluorite solubility [40]. The formation of fluorite minerals in the investigated area is recorded by its high positive relationship with fluoride contents ($r = 0.832$, $p < 0.005$; Table 3). Also, the high positive correlation between fluorite and sellaïte minerals (0.978, $p < 0.005$) along the seawater columns may be accompanied with the formation of ideal fluorite–sellaite solid solution with a composition $Ca_xMg_{(x-1)}F_2$ which would yield a higher equilibrium CaF_2 ion concentration product than pure fluorite [51]. However, the previous study on the hydrothermal fluorite deposition in central Russia that includes zones of fluorite–sellaite aggregated and suggested its formation from the decomposition of the metastable phase $4CaF_2$ $3MgF_2$ [51]. The positive correlation of Mg and HCO_3 ($r = 0.246$, $p < 0.005$; Table 3) may be accompanied with the formation of magnesite ($MgCO_3$). However, during the calcination of dolomite ($CaMg[CO_3]_2$), MgO can be provided and Mg cations substitute Ca cations strictly in its calcined structure [52–54]. Also, MgO in calcined dolomite leads to the formation of CaF_2 after the adsorption of fluoride ion [55].

Interestingly, ANOVA: two factor without replication analysis focuses on the significant effect of both determined parameters ($F_{crit} = 1.26$ and $p < 0.005$) and sampling depths in each location ($F_{crit} = 1.67$ and $p < 0.000$) on the mineral formation. Additionally, the stepwise regression analysis for the determined minerals along the investigated area is expressed in the following significant equations:

$$\text{Calcite} = 0.25 + 1.00\ \textbf{aragonite} - 0.001\ T + 0.01\ \text{fluorite} + 0.002\ \text{Mg} - 0.002\ \text{Ca} - 0.009\ \text{sellaïte}$$

$$\text{Aragonite} = -0.25 + 0.999\ \textbf{calcite} + 0.001T + 1.00\ \text{aragonite} - 0.001T + 0.01\ \text{fluorite} + 0.002\ \text{Mg} - 0.002\ \text{Ca} - 0.009\ \text{sellaite} - 0.002\ \text{Mg} + 0.002\ \text{Ca} - 0.011\ \text{fluorite}$$

$$\text{Dolomite} = -15.30 + 0.661\ \textbf{calcite} + 0.147\ \text{salinity} - 0.131\ T - 0.111\ \text{HCO}_3 - 0.098\ \text{fluorite}$$

$$\text{Fluorite} = -1.02 + 1.011\ \textbf{sellaite} + 0.105\ \textbf{Ca} - 0.092\ \textbf{Mg} + 0.062\ \ \textbf{calcite}$$

$$\text{Sellaite} = 0.88 + 0.919\ \textbf{fluorite} - 0.056\ \textbf{aragonite} - 0.099\ \textbf{Ca} + 0.089\ \textbf{Mg} + 0.062\ \textbf{F}$$

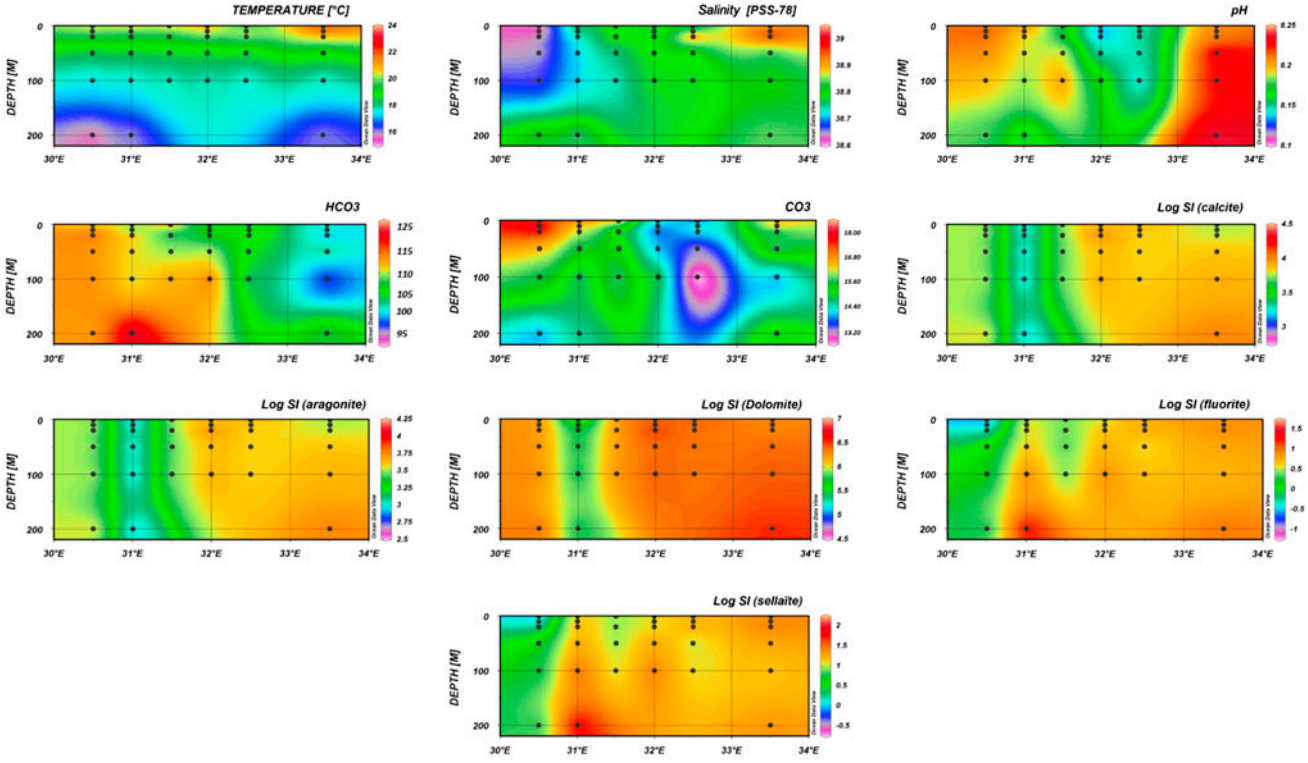

Fig. 3. Vertical distribution of the physicochemical parameters and saturation index (SI) of minerals along the eastern Egyptian Mediterranean Sea coast.

From the previous equations, it is obvious that the formation and dissolution of calcite, aragonite, dolomite and sellaïte minerals are controlled by the fluorite one. Also, calcium and magnesium concentrations in the seawater columns in the investigated hot spots areas affect the precipitation of calcite, aragonite, fluorite and sellaïte minerals. Dolomite is the only mineral that is controlled by the salinity variation which is affected by discharged waters. Moreover, fluoride content plays an important role in the formation of the sellaïte mineral.

4. Conclusion

Some physicochemical parameters, including *T*, salinity, pH, HCO_3, CO_3, Ca, Mg and F, were determined. Ca, Mg and F concentrations were affected by the thrown untreated or primary treated wastes and gave levels different from those recorded for open seawater. The calculated mMg/Ca showed values >2 (2.02–11.12), indicating the formation of aragonite and high-Mg calcite in the marine organisms along the investigated area. Amongst, all the studied sectors, only Rosetta and Damietta regions gave fluoride concentrations relatively similar to the unpolluted seawaters (1.2–1.5 mg/l). Saturation indices (SI) of calcite, aragonite, dolomite, fluorite and sellaïte minerals in the investigated area were evaluated. It seems from the detected values and horizontal and vertical patterns of the saturation indices that calcite, aragonite and dolomite species were formed (SI > 1) along the water columns with ranges of 2.83–4.81, 2.58–4.55 and 0.99–7.33, respectively. Moreover, the distribution patterns of both fluorite and sellaïte minerals were influenced by the discharged waters; however, their trends were similar to the salinity and pH ones. These fluoride minerals seemed to be in equilibrium with their ionic species in the studied sectors. Interestingly, fluoride did not precipitate as the fluorite and sellaïte in the Rosetta and Damietta sectors, the branches of the Nile River, due to its strong tendency to form complexes with other elements stronger than calcium and magnesium ion pairs at the area of seawater estuaries contact. ANOVA: two factor without replication, correlation matrix and stepwise regression model analyses pointed to the change in the physicochemical parameters along the sampling locations owing to the discharged effluents composition. Additionally, the

stepwise regression models confirmed the effect of the discharged waters on the formed minerals along the investigated coastal region. Recalling to this conclusion, the following up of minerals can be used as a good indicator to monitor pollution in the coastal zones of the Egyptian Mediterranean Sea. The pollution by untreated discharged waters can cause harmful effects to the marine ecosystem as well as mankind in the long exposure time. Therefore, the results of this investigation are important to future research and will be used in the effective management of the contaminated regions.

Acknowledgements

Many thanks to the physical oceanography labour, National Institute of Oceanography and Fisheries for providing the data of salinity and temperature.

References

[1] M.S. Masoud, G.F. El-Said, Behavior of some chloride, carbonate, phosphate, sulphate and borate additive salt–NaCl aqueous solution systems in the absence and presence of NaF, Desalin. Water Treat. 29 (2011) 1–9.
[2] E. Ruiz-Agudo, M. Kowacz, C.V. Putnis, A. Putnis, The role of background electrolytes on the kinetics and mechanism of calcite dissolution, Geochim. Cosmochim. Acta 74 (2010) 1256–1267.
[3] M. Kowacz, C.V. Putnis, A. Putnis, The effect of cation: Anion ratio in solution on the mechanism of barite growth at constant supersaturation: Role of the desolvation process on the growth kinetics, Geochim. Cosmochim. Acta 71 (2007) 5168–5179.
[4] M. Wolthers, G. Nehrke, J.P. Gustafsson, P. Van Cappellen, Calcite growth kinetics: Modeling the effect of solution stoichiometry, Geochim. Cosmochim. Acta 77 (2012) 121–134.
[5] M.A. Elrashidi, W.L. Lindsay, Chemical equilibria of fluorine in soils: A theoretical development, Soil Sci. 141 (1986) 275–280.
[6] R. Allmann, Fluorine 9A in Handbook of Geochemistry, vol. II/1, K.H. Wedepohl (Ed.), (published in 1978), Springler-Verlag Berlin Heidelberg, New York, NY, 1974.
[7] R. Liteplo, R. Gomes, P. Howe, Environmental Health Criteria 227, World Health Organization (WHO), Geneva, 2002.
[8] L. Pertti, B. Birgitta, The occurrence and geochemistry of fluorides with special reference to natural waters in Finland, Summary: Geologian tutkimuskeskus, Tutkimusraportti (Geological Survey of Finland, Report of Investigation 149), 2000, 40 p.
[9] K.D. Brahman, T.G. Kazi, H.I. Afridi, S. Naseem, S.S. Arain, N. Ullah, Evaluation of high levels of fluoride, arsenic species and other physicochemical parameters in underground water of two sub districts of Tharparkar, Pakistan: A multivariate study, Water Res. 47 (2013) 1005–1020.
[10] K.D. Brahman, T.G. Kazi, H.I. Afridi, S. Naseem, S.S. Arain, S.K. Wadhwa, F. Shah, Simultaneously evaluate the toxic levels of fluoride and arsenic species in underground water of Tharparkar and possible contaminant sources: A multivariate study, Ecotoxicol. Environ. Saf. 89 (2013) 95–107.
[11] A. Teutli-Sequeira, V. Martínez-Miranda, M. Solache-Ríos, I. Linares-Hernández, Aluminum and lanthanum effects in natural materials on the adsorption of fluoride ions, J. Fluorine Chem. 148 (2013) 6–13.
[12] J.A. Camargo, Fluoride toxicity to aquatic organisms: A review, Chemosphere 50 (2003) 251–264.
[13] G.F. El-Said, N.A. Sallam, The uptake of fluoride concentration and its effects on the growth rate of shrimps (*Palaemon elegans*, Rathke), Chem. Ecol. 24 (2008) 191–205.
[14] K. Larsen, K. Bechgaard, S.L.S. Stipp, The effect of the Ca^{2+} to CO_3^{2-} activity ratio on spiral growth at the calcite {10$\bar{1}$4} surface, Geochim. Cosmochim. Acta 74 (2010) 2099–2109.
[15] J.W. Morse, R.S. Arvidson, The dissolution kinetics of major sedimentary carbonate minerals, Earth Sci. Rev. 58 (2002) 51–84.
[16] G.J. Stockmann, D. Wolff-Boenisch, S.R. Gislason, E.H. Oelkers, Do carbonate precipitates affect dissolution kinetics? 1: Basaltic glass, Chem. Geol. 284 (2011) 306–316.
[17] E.H. Oelkers, S.V. Golubev, O.S. Pokrovsky, P. Bénézeth, Do organic ligands affect calcite dissolution rates? Geochim. Cosmochim. Acta 75 (2011) 1799–1813.
[18] J. Warren, Dolomite: Occurrence, evolution and economically important associations, Earth Sci. Rev. 52 (2000) 1–81.
[19] E. García, P. Alfonso, E. Tauler, S. Galí, Surface alteration of dolomite in dedolomitization reaction in alkaline media, Cem. Concr. Res. 33 (2003) 1449–1456.
[20] E. Busenberg, L.N. Plummer, The kinetics of dissolution of dolomite in CO_2–H_2O systems at 1.5 to 65°C and 0 to 1 atm PCO_2, Am. J. Sci. 282 (1982) 45–78.
[21] D.A. Courtenary, J.R. Rex, The spectrophotometric determination of fluoride in seawater, J. Mar. Res. 12 (1951) 203–314.
[22] M.S. Masoud, W.M. El-Sarraf, A.A. Harfoush, G.F. El-Said, Studies on fluoride-zirconium-alizarin red S reaction, Egypt. Sci. Mag. 1 (2004) 27–32.
[23] APHA-AWWA-WPCF, Standard Methods for the Examination of Water and Waste Water, twentieth ed., American Public Health Association, Washington, DC, 1999.
[24] A.G. Dickson, C.L. Sabine, J.R. Christian, Guide to Best Practices for Ocean CO_2 Measurements, PICES Special Publication, 2007. Available from: http://cdiac.ornl.gov/oceans/Handbook_2007.html.
[25] F. Han, Biogeochemistry of Trace Elements in Arid Environments, Springer, Dordrecht, 2007.
[26] Química General e Inorgánica II, 1º Cuatrimestre de 2009, Material Impreso, Tablas. Available from: http://www.qi.fcen.uba.ar/materias/qi2/%20Backup%20Cuatrimestres%20pasados%20-/2009%202do/guias.html.
[27] G.F. El-Said, M.M. El-Sadawy, A.A. Moneer, Incorporation of fluoride and boron into surface sediments along the Egyptian Mediterranean coast, Egypt. J. Aquat. Res. 36 (2010) 569–583.

[28] G.A. Cole, A Text Book of Limnology, second ed., The C.V. Mosby Company, London, 1979.
[29] G.K. Reid, Ecology and Inland Waters and Estuaries, Reinhold Publishing Corporation (A subsidiary of Champman Reinhold, Inc.), London, 1966.
[30] P. Castro, M.E. Huber, Marine Biology, eighth ed., McGraw-Hill, New York, NY, 2010.
[31] G.F. El-Said, Bioaccumulation of key metals and other contaminants by seaweeds from the Egyptian Mediterranean Sea Coast in relation to human health risk, Hum. Ecol. Risk Assess. 19 (2013) 1285–1305.
[32] D.H. Youssef, G.F. El-Said, A.H. Shobier. Distribution of total carbohydrates in surface sediments of the Egyptian Mediterranean coast, in relation to some inorganic factors, Arabian J. Chem., 7 (2014) 823–832.
[33] J.B. Ries, M.A. Anderson, R.T. Hill, Seawater Mg/Ca controls polymorph mineralogy of microbial $CaCO_3$: A potential proxy for calcite-aragonite seas in Precambrian time, Geobiology 6 (2008) 106–119.
[34] J.B. Ries, Review: Geological and experimental evidence for secular variation in seawater Mg/Ca (calcite-aragonite seas) and its effects on marine biological calcification, Biogeosciences 7 (2010) 2795–2849.
[35] C. Saenger, Z. Wang, Magnesium isotope fractionation in biogenic and abiogenic carbonates: Implications for paleoenvironmental proxies, Quat. Sci. Rev. 90 (2014) 1–21.
[36] C.P. Summerhayes, G. Sestini, R. Misdorp, N. Marks, Nile Delta: Nature and evolution of continental shelf sediments, Mar. Geol. 27 (1978) 43–65.
[37] G. Jacks, P. Bhattacharya, V. Chaudhary, K.P. Singh, Controls on the genesis of some high-fluoride groundwaters in India, Appl. Geochem. 20 (2005) 221–228.
[38] S. Kannan, J.H.G. Rocha, S. Agathopoulos, J.M.F. Ferreira, Fluorine-substituted hydroxyapatite scaffolds hydrothermally grown from aragonitic cuttlefish bones, Acta Biomater. 3 (2007) 243–249.
[39] J. Li, Y. Wang, X. Xie, C. Su, Hierarchical cluster analysis of arsenic and fluoride enrichments in groundwater from the Datong basin, Northern China, J. Geochem. Explor. 118 (2012) 77–89.
[40] K. Tanaka, T. Ono, Y. Fujioka, S. Ohde, Fluoride in non-symbiotic coral associated with seawater carbonate, Mar. Chem. 149 (2013) 45–50.
[41] W.M. El-Sarraf, M.S. Masoud, A.A. Harfoush, G.F. El-Said, Fluoride distribution and the effect of some ions along Alexandria coastal Mediterranean seawater of Egypt, J. Environ. Sci. 15 (2003) 639–646.
[42] G.F. El-Said, Distribution of fluoride content in some localities of Egyptian coastal water, PhD thesis, Chemistry Department, Faculty of Science, Alexandria University, 2005, 358 p.
[43] A. El-Sikaily, G.F. El-Said, Fluoride, some selected elements, lipids, and protein in the muscle and liver tissues of five fish species along the Egyptian Mediterranean Sea Coast, Hum. Ecol. Risk Assess. 16 (2010) 1278–1294.
[44] G.F. El-Said, D.H. Youssef, Accumulation of some trace metals and fluoride in economically important fish species from coastal waters of Alexandria, Egypt during Summer 2006, Egypt. J. Aquat. Res. 35(1) (2009) 21–41.
[45] M.M. El-Sadaawy, G.F. El-Said, Assessment of fluoride in three selected polluted environments along the Egyptian Mediterranean Sea: Effects on local populations, Hum. Ecol. Risk Assess. 20 (2014) 1643–1658.
[46] D.L. Macalady, Perspectives in Environmental Chemistry, Oxford University Press Inc., New York, NY, 1998.
[47] H.H. Teng, P.M. Dove, J.J. De Yoreo, Kinetics of calcite growth: Surface processes and relationships to macroscopic rate laws, Geochim. Cosmochim. Acta 64 (2000) 2255–2266.
[48] D. Dyrssen, M. Wedborg, Chemical Speciation in Estuarine waters, Chemistry and Biogeochemistry of Estuaries, Wiley-Interscience, New York, NY, 1980.
[49] E.D. Goldberg, The Sea, in: Marine Chemistry, vol. 5, John Wiley & Sons, New York, NY, 1974.
[50] C.L. Yang, R. Dluhy, Electrochemical generation of aluminum sorbent for fluoride adsorption, J. Hazard. Mater. 94 (2002) 239–252.
[51] A. Garand, A. Mucci, The solubility of fluorite as a function of ionic strength and solution composition at 25°C and 1 atm total pressure, Mar. Chem. 91 (2004) 27–35.
[52] S. Karaca, A. Gürses, M. Ejder, M. Acikyildiz, Adsorptive removal of phosphate from aqueous solutions using raw and calcinated dolomite, J. Hazard. Mater. 128 (2006) 273–279.
[53] X. Qiu, K. Sasaki, T. Hirajima, K. Ideta, J. Miyawaki, Temperature effect on the sorption of borate by a layered double hydroxide prepared using dolomite as a magnesium source, Chem. Eng. J. 225 (2013) 664–672.
[54] E.P. Solotchina, E.V. Sklyarov, P.A. Solotchin, E.G. Vologina, V.N. Stolpovskaya, O.A. Sklyarova, N.N. Ukhova, Reconstruction of the Holocene climate based on a carbonate sedimentary record from shallow saline Lake Verkhnee Beloe (*western Transbaikalia*), Russ. Geol. Geophys. 53 (2012) 1351–1365.
[55] K. Sasaki, M. Yoshida, B. Ahmmad, N. Fukumoto, T. Hirajima, Sorption of fluoride on partially calcined dolomite, Colloids Surf. A 435 (2013) 56–62.
[56] S.S. Hassan, Impact of flash floods on the hydrogeological aquifer system at Delta Wadi El-Arish (North Sina), in: Fifteenth International Water Technology Conference, IWTC-15, Helnan Palestine Hotel, Alexandria, 2011, 28–30 May, 2011. Available from: http://iwtc.info/archive/iwtc-2011/.